Supporting Information for

High cationic dispersity boosted oxygen reduction reactivity in multi-element doped perovskites

Li *et al.*

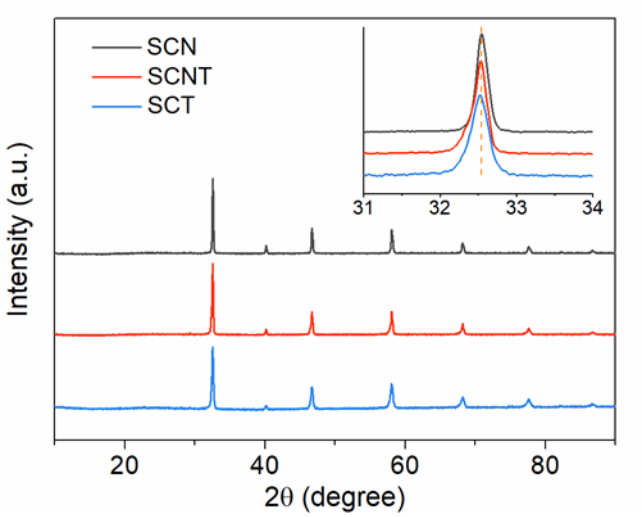

Supplementary Figure 1 X-ray diffraction data of SCN, SCNT, and SCT samples. Data are shown as a line and offset in y for clarity. The vertical dashed line in the inset is a guide to the eye.

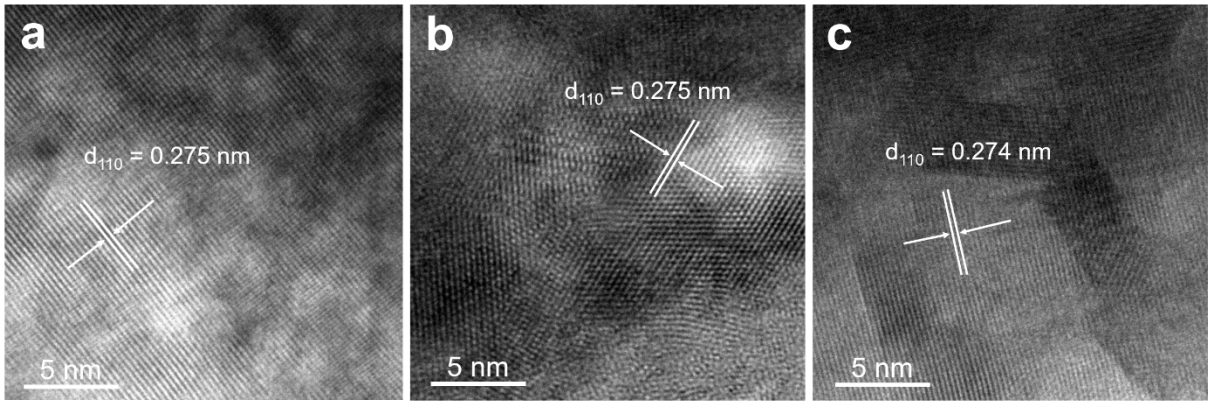

Supplementary Figure 2 HRTEM images of (**a**) SCN, (**b**) SCNT, and (**c**) SCT.

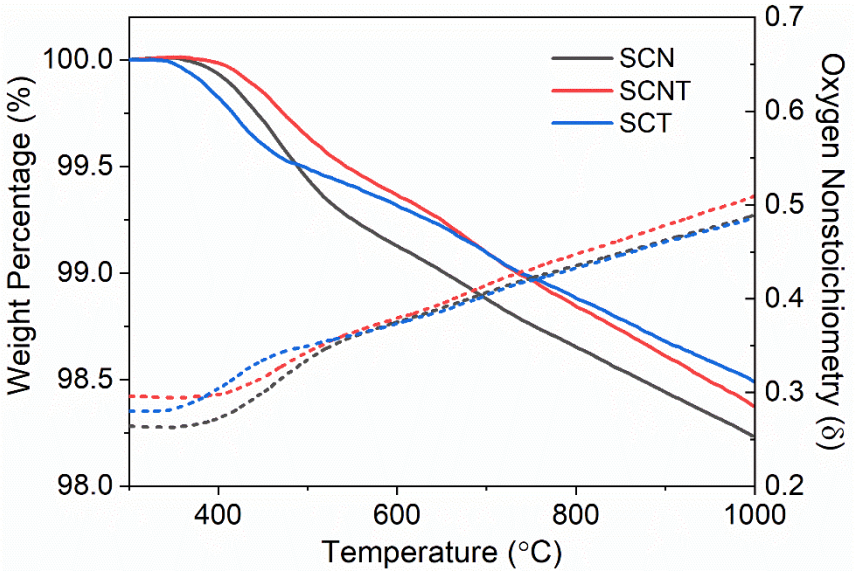

Supplementary Figure 3 Mass and oxygen nonstoichiometry change of SCN, SCT, and SCNT, determined using thermogravimetry in flowing N_2 with a flow rate of 20 $mL \cdot min^{-1}$.

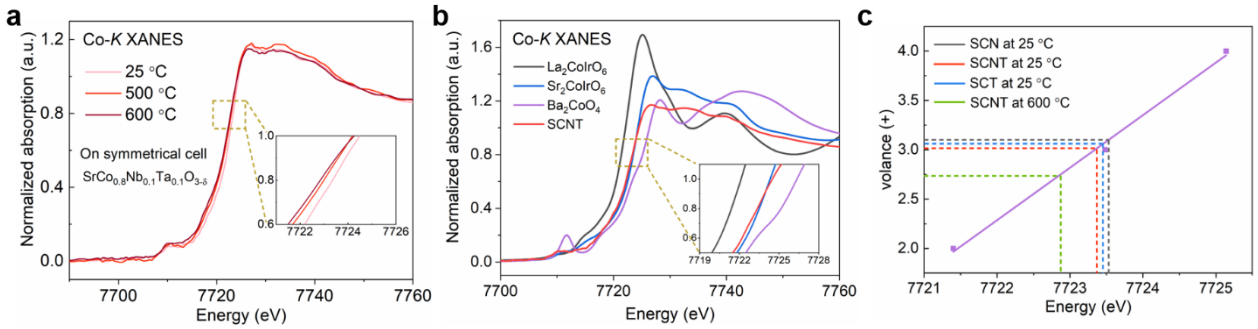

Supplementary Figure 4 (**a**) Co K-edge XANES data of SCNT at different temperature. (**b**) Co K-edge XANES data of SCNT (red line) and standards for Co^{2+} (gray line), Co^{3+} (blue line), and Co^{4+} (purple line). (**c**) Co average valence calculated from the absorption edge shift in XANES data of SCN, SCNT, and SCT.

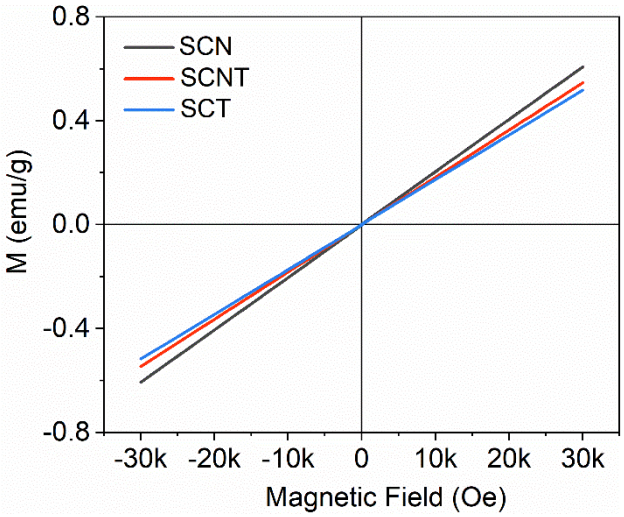

Supplementary Figure 5 Field dependence of the magnetization of SCN, SCNT, and SCT.

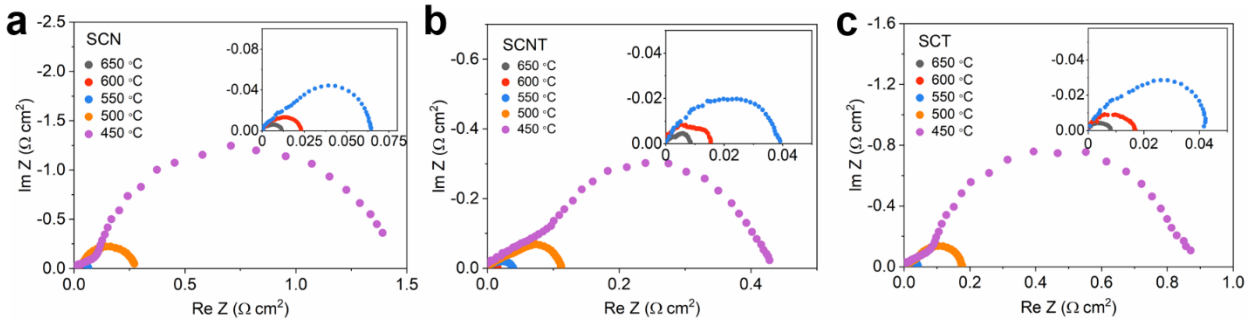

Supplementary Figure 6 Nyquist plots of temperature dependent electrochemical impedance of (**a**) SCN, (**b**) SCNT, and (**c**) SCT.

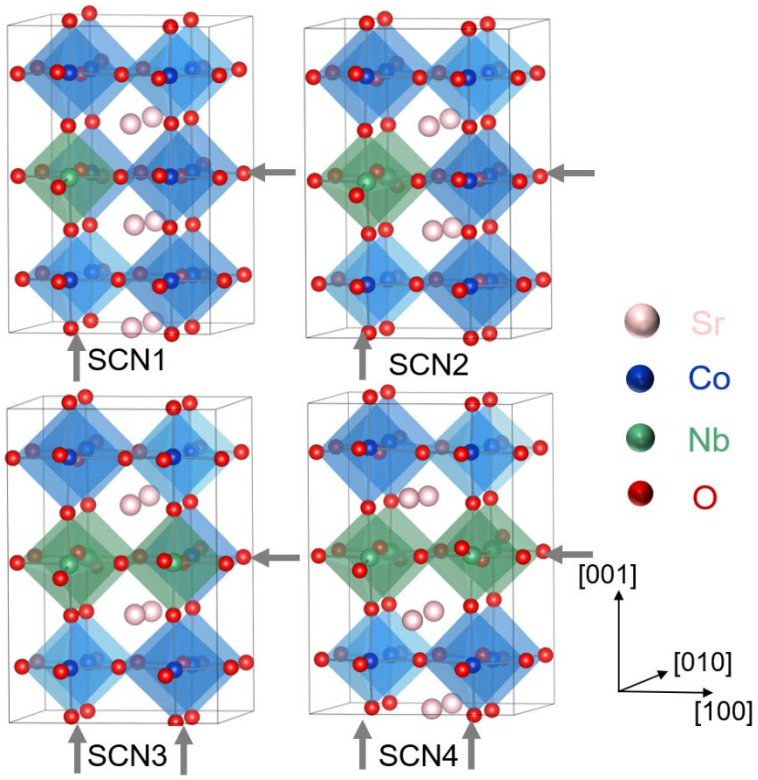

Supplementary Figure 7 DFT models of SCN with different degrees of cation aggregation. Arrows indicate the direction through which planes intercept (four planes along the [100] and six planes along the [001]).

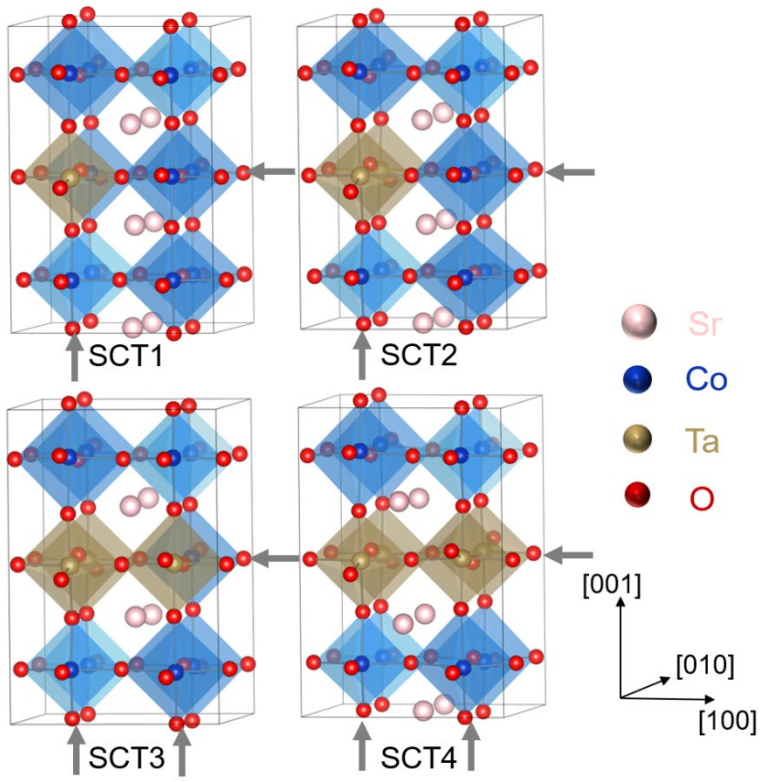

Supplementary Figure 8 DFT models of SCT with different degrees of cation aggregation. Arrows indicate the direction through which planes intercept (four planes along the [100] and six planes along the [001]).

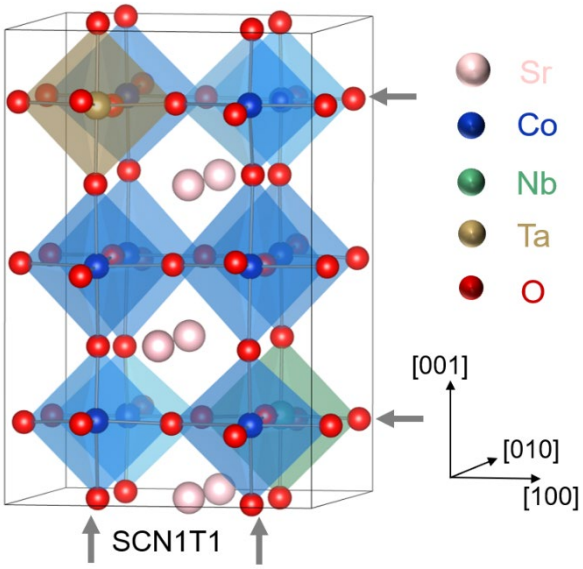

Supplementary Figure 9 DFT model of SCNT. Arrows indicate the direction through which planes intercept (two planes along [100] and two planes along [001]).

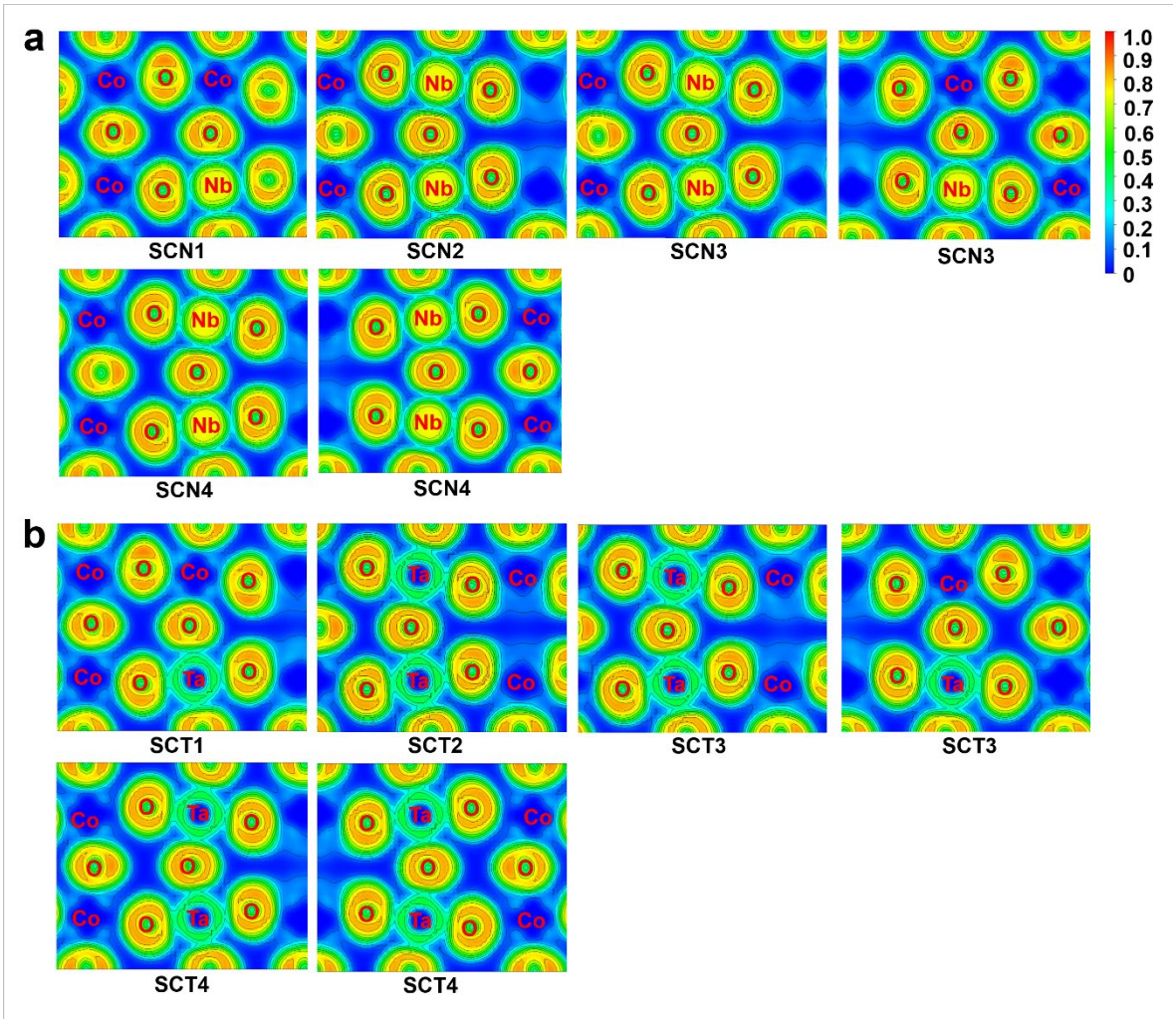

Supplementary Figure 10 ELF maps of the (100) plane of (**a**) SCN and (**b**) SCT systems. The BO_6 octahedron contains eight *B*-O bonds, the ELF values for which are obtained by combining the ELF values for the (100) and (001) planes.

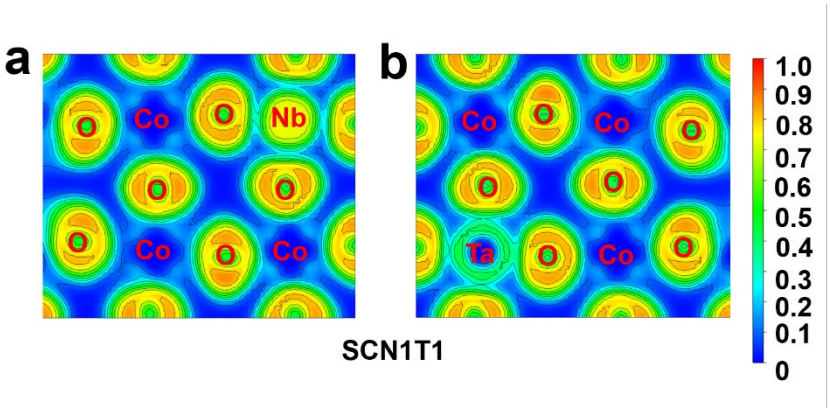

Supplementary Figure 11 ELF map for the (100) plane for **(a)** Nb-O and **(b)** Ta-O.

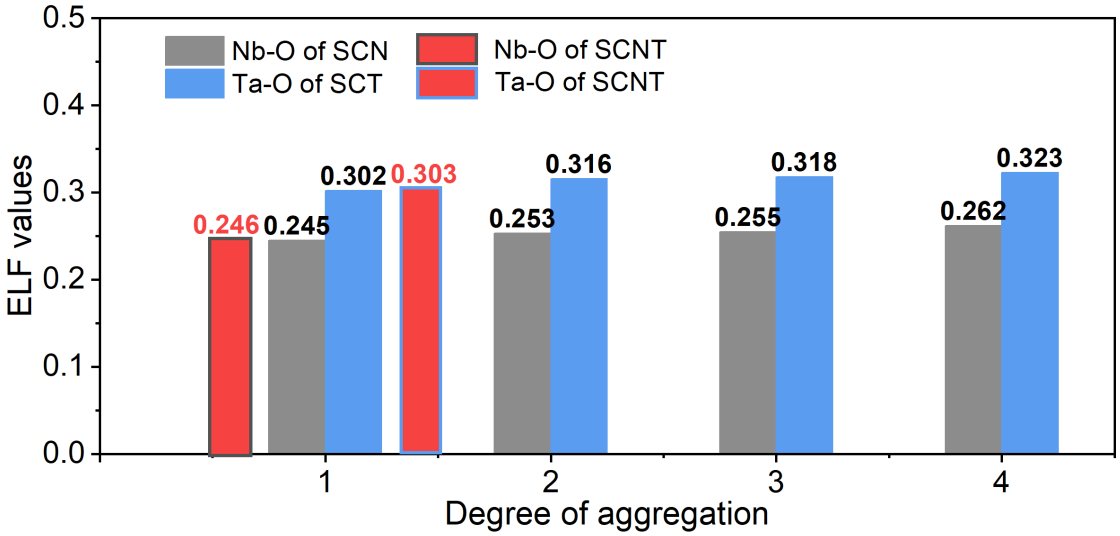

Supplementary Figure 12 ELF values along Nb-O and Ta-O bonds as a function of cation aggregation for models in **Supplementary Figures 7-9**, "degree of aggregation" is the dopant concentration in 2 × 2 × 3 supercells of $SrCoO_3$.

Supplementary Note 1

SCN, SCNT, and SCT samples are all cubic perovskites with formula ABO_3, for which the free lattice volume is calculated:

$$V_f = V - \frac{4}{3}\pi {r_A}^3 - \frac{4}{3}\pi {r_B}^3 - 3 \times \frac{4}{3}\pi {r_O}^3$$

where V_f is the free lattice volume, V is the lattice volume, r_A is the radius of the A-site ion, r_B is the radius of the B-site ion, and r_O is the radius of oxygen ion. Ionic radii are based on work by Shannon and Jia [1,2], where the ionic radius for Sr^{2+} with 12-fold coordination is 1.44 Å, the ionic radius for Co^{3+}, Nb^{5+}, and Ta^{5+} with 6-fold coordination are 0.61, 0.64, and 0.64 Å, respectively, and the ionic radius for O^{2-} is 1.4 Å. Other values are obtained from joint Rietveld refinement using powder diffraction data.

V_f (SCN)

$= 59.503 – 4/3 \times (\pi \times 1.44^3 + (0.8 \times \pi \times 0.61^3 + 0.2 \times \pi \times 0.64^3) + 3 \times \pi \times 1.4^3)$

$= 11.44$ Å^3

V_f (SCNT)

$= 59.415 – 4/3 \times (\pi \times 1.44^3 + (0.8 \times \pi \times 0.61^3 + 0.1 \times \pi \times 0.64^3 + 0.1 \times \pi \times 0.64^3) + 3 \times \pi \times 1.4^3)$

$= 11.53$ Å^3

V_f (SCT)

$= 59.584 – 4/3 \times (\pi \times 1.44^3 + (0.8 \times \pi \times 0.61^3 + 0.2 \times \pi \times 0.64^3) + 3 \times \pi \times 1.4^3)$

$= 11.61$ Å^3

Supplementary Note 2

Regions around O in red have the largest ELF value of ca. 0.830, revealing a high localization of electrons, consistent with lone pair electrons that attract electrons from adjacent metal atoms. Regions around Co atoms are blue, demonstrating a high delocalization of electrons, indicative of ionic bonding between Co and O. [10] The largest ELF value along Nb-O bonds is larger than for that along Co-O bonds, indicating that electrons are more localized between O and Ta than between O and Co, demonstrating a higher covalency of Nb-O than Co-O. Similarly, **Figure 6b** and **Figure S8b** reveal stronger covalency of Ta-O than Co-O.

Composition: $SrCo_{0.8}Nb_{0.105}Ta_{0.095}O_{2.562}$, density: 5.6525 g cm^{-3}, space group: $Pm\bar{3}m$, lattice parameter: a = 3.90402(3) Å.

Atom	Site	x	y	z	Occupancy	U_{iso} (Å^2)
Sr	1*b*	0.5	0.5	0.5	1.000 (fixed)	0.01714(26)
Co	1*a*	0	0	0	0.800(fixed)	0.01004(21)
Nb	1*a*	0	0	0	0.105(fixed)	0.01004(21)
Ta	1*a*	0	0	0	0.095(fixed)	0.01004(21)
O	3*d*	0.5	0	0	0.851(4)	0.01992(61)

The weighted profile reliability factor wRp using SXRD, NPD-154, and NPD-241 data is 2.96%, 7.43%, and 7.53%, respectively. When refining the occupancy of O, the occupancy of the *B*-site cation was fixed. The occupancy of the *B*-site cation has been refined when the oxygen occupancy was unity.

Composition: $SrCo_{0.846}Nb_{0.154}O_{2.565}$, density: 5.4515 g cm^{-3}, space group: $Pm\bar{3}m$, lattice parameter: a = 3.90357(3) Å

Sr	1*b*	0.5	0.5	0.5	1.000 (fixed)	0.01336(47)
Co	1*a*	0	0	0	0.846(9)	0.01336(57)
Nb	1*a*	0	0	0	0.154(9)	0.01336(57)
O	3*d*	0.5	0	0	0.855(6)	0.01945(50)

wRp using SXRD, NPD-154, and NPD-241 data = 2.11%, 7.42% and 7.66%, respectively.

Composition: $SrCo_{0.805}Ta_{0.195}O_{2.589}$, density: 5.9728 g cm^{-3}, space group: $Pm\bar{3}m$, lattice parameter: a = 3.90820(4) Å

Sr	1*b*	0.5	0.5	0.5	1.000 (fixed)	0.01700(23)
Co	1*a*	0	0	0	0.805(2)	0.01028(18)
Ta	1*a*	0	0	0	0.195(2)	0.01028(18)
O	3*d*	0.5	0	0	0.863(5)	0.01230(67)

wR using SXRD, NPD-154 data, NPD-241 data = 3.58 %, 5.36% and 7.90%, respectively.

Supplementary Table 1 Refined crystallographic details of the SCNT, SCN, and SCT

sample using the synchrotron X-ray (SXRD) and neutron powder diffraction data at neutron wavelengths of approximately 1.54 Å (NPD-154) and 2.41 Å (NPD-241).